Preliminary Report of De Novo Adipogenesis Using Novel Bioabsorbable Implants and Image Evaluation Using A Porcine Model

Shuichi Ogino (sogino12@belle.shiga-med.ac.jp)
Shiga University of Medical Science
Atsushi Yamada
Shiga University of Medical Science
Yusuke Kambe
National Cerebral and Cardiovascular Center
Takashi Nakano
Kyoto University
Sunghee Lee
Kyoto University
Michiharu Sakamoto
Kyoto University
Yuki Kato
Gunze QOL Research Center Laboratory
Saki Okumura
Gunze QOL Research Center Laboratory
Junko Okano
Shiga University of Medical Science
Koji Yamauchi
Gunze QOL Research Center Laboratory
Yoshihisa Suzuki
Shiga University of Medical Science
Tetsuji Yamaoka
National Cerebral and Cardiovascular Center
Naoki Morimoto
Kyoto University

Research Article

Keywords: MRI, ultrasound, 3D surface imaging, adipose tissue, evaluation, material

Posted Date: March 6th, 2021

DOI: https://doi.org/10.21203/rs.3.rs-275434/v1

Version of Record: A version of this preprint was published at Journal of Artificial Organs on March 2nd, 2022. See the published version at https://doi.org/10.1007/s10047-022-01313-8.

Abstract

Our bioabsorbable poly-L-lactic acid (PLLA) mesh implants containing collagen sponge is replaced with adipose tissue after implantation and is an innovative method for breast reconstruction. We investigated the formation of adipose tissue in a porcine model and evaluated the process via multimodal images in this preliminary study using an implant aggregate to generate the larger adipose tissue. The implant aggregate consists of PLLA mesh implants containing collagen sponge and a poly-glycolic acid woven bag covering them. We inserted the implant aggregates under the porcine mammary glands. Magnetic resonance imaging (MRI), ultrasonography (USG), and 3D surface imaging, and histological evaluations were performed to evaluate the formation of adipose tissue over time. The volume of the implant aggregate and the formed adipose tissue inside the implant aggregate could be evaluated over time via MRI. The space within the implant aggregate was not confirmed on USG due to the acoustic shadow of the PLLA threads. The change in volume was not confirmed precisely using 3D surface imaging. Histologically, the newly-formed adipose tissue was confirmed on the skin side. This implant aggregate has the ability to regenerate adipose tissue, and MRI is an appropriate method for the evaluation of the formation of adipose tissue.

Introduction

The number of breast cancer patients is increasing, and several patients suffer from the psychological burden of a mastectomy. This has led to an increasing number of patients desiring breast reconstruction. Currently, reconstruction of the breast is performed via autologous tissue transfer, an artificial implant, and autologous fat transfer. The key components of aesthetic outcomes of breast augmentation are breast symmetry, size, and shape[1], and many techniques are reported to minimize operative complications while maximizing aesthetic appearance[2–5]. However, after breast reconstruction or breast augmentation, the size and shape of the reconstructed breast gradually change due to detumescence or atrophy. Therefore, evaluation of the reconstructed breast over time is required.

Both magnetic resonance imaging (MRI) and 3-dimensional (3D) surface imaging are accurate and reliable methods to assess the breast volume[2,6,7]. Precise estimates of breast volume and detection of soft tissue can be achieved via MRI. However, repeated MRIs are not practical or cost-effective. In contrast, 3D surface imaging is able to be performed in an outpatient setting, making it less of a burden on the patient[8–10]. In a previous *in vivo* study, we confirmed the formation of adipose tissue using ultrasound imaging in the internal space of polypropylene mesh containing a collagen sponge (CS) one year after implantation[11].

We developed an innovative method of breast reconstruction using a bioabsorbable implant that is substituted by newly-formed adipose tissue after implantation without the use of growth factors or cells[12,13]. This implant aggregate consists of a poly-L-lactic acid (PLLA) mesh implant containing CS. The maintenance of the internal space *in vivo* for approximately one year after implantation is essential for the formation of adipose tissue using this PLLA implant in a rodent model[13]. However, the amounts

of formed adipose tissue in rodent and rabbit models were not sufficient to fill the volume required for breast augmentation following clinical mastectomy[12,13].

In this study, we inserted a PLLA implant aggregate enveloped with a poly-glycolic acid (PGA) mesh bag into the abdomen under the mammary gland using a porcine model. In this preliminary study, we evaluated the adipogenesis within this implant aggregate and investigated the efficacy of MRI, ultrasonography, and 3D surface imaging as evaluation methods of the adipogenesis over time.

Results

MRI findings

The MRIs are shown in Figure 1. In the T1-weighted image (T1WI), the normal adipose tissue and the implant aggregate were able to be distinguished at all time points. The newly-formed adipose tissue was identified as a high-intensity lesion in T1WI images and a low-intensity lesion in water excitation (WE) images. It was confirmed to be inside the implant aggregate especially at the skin side and in contact with the original porcine fat at 3 and 6 months after implantation. The time course of the volume of the implant aggregate and the formed adipose tissue inside the implant aggregate are shown in Table 1. The volume of the implant aggregate gradually decreased over time while the volume of adipose tissue inside the implant aggregate gradually increased over time. The newly-formed adipose tissue occupied approximately 22% of the implant aggregate volume.

Ultrasonographic findings

The ultrasonographic findings are shown in Figure 2. The outer surface of the implant aggregate was hyperechoic immediately after implantation and was clearly defined. However, at 1, 3, and 6 months after implantation, the outer surface of the implant aggregate was not clearly defined. The ultrasonic observation of the internal space of the implant aggregate was disturbed by the acoustic shadow of the PLLA thread and PGA mesh immediately after implantation. At 1, 3, and 6 months after implantation, the acoustic shadow was diminished, and a hyperechoic area that represented the newly-formed tissue or the PLLA thread was identified at the skin side of the implant aggregate.

3D surface imaging findings

The 3D surface images are shown in Figure 3a. At 1, 3, and 6 months after implantation, a slight bulge was observed at the abdominal surface. The pre- and post-implantation images are compared in Figure 3b. The volume at the abdominal surface increased 33.15 cm^3 immediately after implantation.

Histological assessment of the newly-formed tissues

Micrographs of hematoxylin-eosin (H&E)-stained sections, oil-red-o-stained sections, and azocarmine and aniline blue (AZAN)-stained sections are shown in Figures 4a, b, and c, respectively. The presence of PLLA mesh was confirmed histologically at six months after implantation. The internal space in the implant

aggregate was maintained until six months after implantation, and the newly-formed tissue inside the implant aggregate consisted of adipose tissue on the skin side and collagen fiber elsewhere. A micrograph of anti-CD31 stained sections is shown in Figure 4d. The formation of capillaries was confirmed both in the area of the newly-formed adipose tissue and in the area of formed collagen fiber.

The average internal area of the implant aggregate was 206.2 mm^2, and that range was 126.9-267.1 mm^2. The average area of newly-formed adipose tissue was 65.4 mm^2, and that range was 31.8-83.6 mm^2.

Discussion

The formation of adipose tissue inside the implant aggregate was evaluated and methods of the evaluation of adipogenesis were investigated using a porcine model. Newly-formed adipose tissue was confirmed to be inside the implant aggregate at six months after implantation. MRI was determined to be an appropriate tool for the evaluation of the volume of the implant aggregate and the formation of adipose tissue.

Adipose tissue has been reported to regenerate with the combination of a bioabsorbable scaffold, growth factors, and/or cells, such as adipose-tissue-derived stromal cells (ASCs) or mature adipocytes[14–20]. Mechanical force also affects adipogenesis, and an *in vitro* study reported that adipogenesis from ASCs is inhibited by mechanical compressive force[21] or mechanical stretch[22]. In our previous *in vivo* study, we reported the importance of maintaining the internal space for adipogenesis[12,13]. Large volumes of adipose tissue were regenerated via an autologous fat transfer using bioabsorbable, polycaprolactone-based scaffolds in a porcine model[23] and poly-4-hydroxybutyrate mesh scaffolds clinically[24]. However, our implant aggregate has the ability to promote de novo adipogenesis without the addition of growth factors or cells. Therefore, that is the novel bioabsorbable implant aggregate.

MRI is a non-invasive imaging method that does not expose patients to radiation and provides superior images compared to computed tomography. MRI is useful for the detection of soft tissue. In this porcine model study, we found that MRI was an effective method for the evaluation of the volume of the implant aggregate over time and for the confirmation of the newly-formed adipose tissue inside the implant aggregate. However, the rates of adipose tissue generation inside the implant aggregate measured via MRI and histological evaluations differ. In next study, we need to investigate the accuracy of the volume of the newly-formed adipose tissue inside the implant aggregate with a larger sample size.

Ultrasonography is an easy-to-use imaging method. In this study, all tissues inside the implant aggregate were not confirmed within six months after the implantation due to the acoustic shadow of the PLLA thread and the PGA mesh on ultrasound. In our previous report, the space or the formed adipose tissue inside the polypropylene mesh was confirmed using ultrasound imaging after implantation[11]. These contrasting results may be due to the difference of the material or thickness of thread in the two studies. In phosphate-buffered saline at 37° C,PLLA was degraded to 50% by weight within two years and PGA

was completely degraded within two to three months[25]. This implant needs to be filled with the formed adipose tissue inside at least one year[12,13]. Therefore, in the next experiment, we need to investigate the regeneration of adipose tissue over a year after implantation using ultrasonography.

The time course of the survival rate of transferred adipose tissue after breast reconstruction and breast augmentation can be evaluated using 3D surface imaging[26]. During 3D surface imaging of the breast, it is essential that the body size does not change during the observation period and that the sternum and costal cartilage are used as deep organ markers. In this porcine model, the implantation was performed in the abdomen due to the lack of sufficient space in the breast and the lack of thick adipose tissue mimicking the mammary gland in the back. However, in the abdomen, this implant aggregate protrudes to the outside and the abdominal cavity. In addition, as the body size increases, the adipose tissue becomes thicker. Therefore, the data regarding the original volume of the implant aggregate and the change in volume over time was not available in this study.

The ultimate goal of this study was to investigate the correlation between the volume of the implant aggregate and the newly-formed adipose tissue. While the volume of the implant aggregate decreased over time as the PGA and PLLA components were absorbed, and the newly-formed adipose tissue was histologically 36% of the volume of the implant aggregation. Angiogenesis is an important factor for the tissue regeneration. In this study, at six months after operation, the adipose tissue was regenerated from the skin side, and newly-formed capillaries were found in the collagen fiber within the implant aggregate. A future study with a larger sample size and a longer follow-up is required.

In conclusion, our novel implant aggregate promotes the formation of adipose tissue. The volume of the implant aggregate and the adipose tissue can be evaluated using MRI.

Methods

Ethics approval

The animals in this study were maintained at the Research Center for Animal Life Science, Shiga University of Medical Science. The experimental protocol was approved by the Institutional Animal Care and Usage Committee at Shiga University of Medical Science (Permit Number: 2019-7-10 (H3)) and was in accordance with the ARRIVE guidelines. The number of animals used in this study was kept to a minimum and all efforts to reduce animal suffering were made in accordance with the protocols established by the Research Center for Animal Life Science of Shiga University of Medical Science.

Preparation of the bioabsorbable implants

The PLLA mesh implant containing CS (PELNAC®, Gunze Ltd., Tokyo, Japan) was prepared in a prolate spheroidal shape as previously reported[13]. Each columnar mesh was 1 cm in diameter and 1 cm in height and was knitted using a 2–0 PLLA thread (Gunze Ltd.). One side of the mesh was closed using purse string sutures. After tightly packing the mesh with 40 mm x 20 mm x 3 mm CS with a porosity of

80–95%, the other end of the mesh was closed using purse string sutures. The polar diameter of the implant was approximately 18 mm, and the greatest equatorial diameter of the implant was approximately 7.5 mm. The implants had multiple 1.5-mm square openings.

Next, 12- 0.015-mm thick PGA multi-filaments were woven into an envelope-shaped bag. We prepared two flat PGA-woven bags that were 110 mm x 35 mm. Thirty pieces of the implant were packed into each PGA woven bag, and two pieces of the implant aggregate were shaped into a cylinder with a diameter of 2.4 cm and a height of 9.0 cm (Figure 5).

Animal experiment

1. Experimental design and operative procedure

A minipig, CLAWN miniature swine, was chosen for this study due to its large body surface and skin that is similar to human skin. One 10-month-old female CLAWN miniature swine was purchased from the Kagoshima Miniature Swine Research Center. After a 2-week preservation period, the minipig weighed 26.3 kg. The animal was cared for as outlined in the Public Health Services Policy on Humane Care and Use of Laboratory Animals. General symptoms such as feeding status and limping were assessed daily.

The minipig was not fed overnight prior to the implantation. Sedation was achieved via an intramuscular injection of 25 mg/kg ketamine (KETALAR®, DAIICHI SANKYO Co., Ltd., Tokyo, Japan) and 0.02 mg/kg medetomidine (DOMITOR®, Nippon Zenyaku Kogyo Co., Ltd., Fukushima, Japan). After sedation, a peripheral intravenous line and a tracheal tube were inserted. The minipig's SpO_2 was monitored, and the minipigs were anesthetized by the inhalation of a mixture of air and oxygen containing 2.0 - 2.5% isoflurane. After shaving the abdominal region, a 6-cm midline incision was made in the abdomen starting 1 cm caudal to the umbilicus (Figure 3a). Next, the fat tissue was incised, and a pocket was prepared over the fascia on each side of the abdomen. Once the implant aggregates were placed into the pockets, the fat and skin were closed with 2-0 blade nylon sutures (Nurolon: Johnson & Johnson K.K., Tokyo, Japan). After this study period, the minipig was used for an additional study.

2. Evaluation of the implant aggregates

The area of implantation and the appearance of the implant aggerates were evaluated under general anesthesia using MRI, ultrasound, and 3D surface imaging prior to implantation, immediately after implantation, and 1, 3, and 6 months after implantation. The tissue from just below the skin to the fascia, including the implant aggregate, on the right side of the abdomen was harvested six months after implantation. The implant aggregate in the left side of the abdomen was preserved for the next study.

2.1. MRI procedure

The minipig was placed on the examination table in the MRI room in the supine position. The mini pig's abdominal part was scanned by a wide-bore 3 Tesla (T) MRI scanner (Magnetom Verio 3T, Siemens Healthcare, Erlangen, Germany) using a dedicated 4ch large flex coil. The scan acquired WI and WE

images in the transverse plane using T1-weighted Dixon imaging (TR/TE = 5.26/2.46 ms; flip angle = 10°; acquisition matrix = 352 × 172; field of view (FOV) = 285 × 350 mm2; slice thickness = 1.0 mm). During the scanning, breathing was controlled using an intravenous injection of 0.4 mg/kg rocuronium bromide (ESLAX®, MSD K.K., Tokyo, Japan). The obtained images were loaded to 3D slicer[27], a software package for the analysis of medical images, in order to calculate the volume of the implant aggregate and the volume of the newly-formed adipose tissue inside the implant aggregate.

2.2. Ultrasonography protocol

An ultrasonographic system (ACUSON S2000 HELX Evolution: Siemens Healthcare K.K., Tokyo, Japan) with a 9L4 probe were used to evaluate the tissue formation inside the implant aggregate.

2.3. Three-dimensional surface imaging protocol

Three-dimensional surface images were obtained using 3D imaging solution (Vectra H2: Integral Corporation., Tokyo, Japan). The volume change of the implantation area between pre- and post-implantation was assessed from the cranial edge of the umbilicus to the inguinal ligament (Figure 3b).

3. Histological assessment of the newly-formed tissues inside the implant aggregate

The harvested specimen was fixed with 4% paraformaldehyde phosphate buffer solution (FUJIFILM Wako Pure Chemical Corporation, Osaka, Japan). The specimen was divided into four equal blocks along the long axis of the implant aggregate. The second block from the caudal side was embedded in optimum cutting temperature compound (Sakura Fine Technical Co. Ltd., Tokyo, Japan) and frozen in ethanol dry ice prior to oil-red-o staining. The three remaining blocks were paraffin-embedded for subsequent H&E, AZAN, and immunohistochemical staining. The 16-μm-thick frozen section from the central region of the tissues was prepared for oil-red-o staining. The 5-μm-thick sections from three aspects of the specimen were prepared for H&E, and the 5-μm-thick sections at the central aspects of the specimen were prepared for AZAN and immunohistochemical staining. Immunohistochemical staining of CD31 was performed to evaluate the formation of new capillaries in the newly-formed tissue. After the deparaffinization and rehydration of the 5-mm-thick paraffin sections, they were immersed in diluted target retrieval solutions (415211; Nichirei Biosciences Inc., Tokyo, Japan) and incubated for 20 min at 98° C. After being cooled to room temperature, the sections were rinsed once in distilled water and immersed in 3% hydrogen peroxide (FUJIFILM Wako Pure Chemical Industries Ltd.) and methanol (FUJIFILM Wako Pure Chemical Industries Ltd.) for 10 min to block endogenous peroxidase activities. The sections were then rinsed in distilled water and 50 mM Tris-HCl buffered saline (Takara Bio Inc., Kusatsu, Japan) with 0.05% Tween 20 (FUJIFILM Wako Pure Chemical Industries Ltd.) and 0.15 M NaCl (TBST). To block nonspecific protein binding, 3% bovine serum albumin (BSA) diluted with phosphate buffered saline (PBS) was applied for 60 min at room temperature. A monoclonal mouse anti-rabbit CD31 antibody (ab182981: Abcam plc., Tokyo, Japan) was applied as the primary antibody at a dilution of 1:10,000 using 1% BSA in PBS and incubated overnight at 4° C. The sections were rinsed in TBST. Next, a peroxidase-labeled secondary antibody (rabbit anti-goat simple stain MAX PO [R]; Histofine; Nichirei

Biosciences Inc.) was applied for 30 min at room temperature. Sections were then rinsed with TBST and exposed to 3,30-diaminobenzidine tetrahydrochloride (Dako Japan Co., Ltd., Tokyo, Japan) for 5 min at room temperature and counterstained with hematoxylin. All microphotographs were obtained using a light microscope (IX83: Olympus corporation, Tokyo, Japan) at 40x magnification. The newly-formed tissues and the newly-formed adipose tissue inside each implant were evaluated on the microphotographs of the H&E stained-sections using ImageJ software version 1.53 g (National Institutes of Health, Bethesda, Maryland, USA). The data were expressed as mean and range.

Declarations

Data Availability Statement

The datasets used and/or analyzed during the current study are available from the corresponding author on reasonable request.

Acknowledgments

This work was partially supported by JSPS KAKENHI (Grant Number JP19K18926) and AMED (Grant Number JP19hm0102068). We would also like to thank Khiem Tran Dang and Tohru Tani for providing general anesthesia, Mayumi Kunimatsu for assistance, and Editage (www.editage.com) for English language editing.

Author contributions:

ShO and NM contributed to the study conception and design. YukK, SaO, and KY prepared the materials and ShO, AY, YusK, TN, SL, MS, YukK, SaO, JO, TY, and NM performed the research. YusK, MS, YS, and TY analyzed data. ShO and NM wrote the first draft of the manuscript and all authors commented on subsequent versions of the manuscript. All authors read and approved the final manuscript. ShO is the grant recipient for JSPS KAKENHI (Grant Number JP19K18926) and NM is the grant recipient for AMED (Grant Number JP19hm0102068).

Conflict of Interest Statement

The authors report no proprietary or commercial interest in any product mentioned or concept discussed in this article.

References

1. Yang, J., Zhang, R., Shen, J., Hu, Y. & Lv, Q. The Three-Dimensional Techniques in the Objective Measurement of Breast Aesthetics. *Aesthetic plastic surgery* **39**, 910–915, doi:10.1007/s00266-015-0560-2 (2015).
2. Choi, M. *et al.* The volumetric analysis of fat graft survival in breast reconstruction. *Plastic and reconstructive surgery.* **131**, 185–191 https://doi.org/10.1097/PRS.0b013e3182789b13 (2013).

3. Fedorov, A. *et al.* 3D Slicer as an image computing platform for the Quantitative Imaging Network. *Magn Reson Imaging.* **30**, 1323–1341 https://doi.org/10.1016/j.mri.2012.05.001 (2012).
4. Farhadi, J., Maksvytyte, G. K., Schaefer, D. J., Pierer, G. & Scheufler, O. Reconstruction of the nipple-areola complex: an update. *Journal of plastic, reconstructive & aesthetic surgery : JPRAS* **59**, 40–53, doi:10.1016/j.bjps.2005.08.006 (2006).
5. Corduff, N. & Taylor, G. I. Subglandular breast reduction: the evolution of a minimal scar approach to breast reduction. *Plastic and reconstructive surgery* **113**, 175–184, doi:10.1097/01.PRS.0000095945.27892.48 (2004).
6. Isogai, N. *et al.* Quantitative analysis of the reconstructed breast using a 3-dimensional laser light scanner. *Ann Plast Surg* **56**, 237–242, doi:10.1097/01.sap.0000200716.82945.b2 (2006).
7. Tepper, O. M. *et al.* Mammometrics: the standardization of aesthetic and reconstructive breast surgery. *Plastic and reconstructive surgery* **125**, 393–400, doi:10.1097/PRS.0b013e3181c4966e (2010).
8. Herold, C., Ueberreiter, K., Busche, M. N. & Vogt, P. M. Autologous fat transplantation: volumetric tools for estimation of volume survival. A systematic review. *Aesthetic plastic surgery* **37**, 380–387, doi:10.1007/s00266-012-0046-4 (2013).
9. Rieger, U. M. *et al.* Does abdominoplasty with liposuction of the love handles yield a shorter scar? An analysis with abdominal 3D laser scanning. *Ann Plast Surg* **61**, 359–363, doi:10.1097/SAP.0b013e31816d824a (2008).
10. Chiu, C. H. Does Stromal Vascular Fraction Ensure a Higher Survival in Autologous Fat Grafting for Breast Augmentation? A Volumetric Study Using 3-Dimensional Laser Scanning. *Aesthetic surgery journal / the American Society for Aesthetic Plastic surgery* **39**, 41–52, doi:10.1093/asj/sjy030 (2019).
11. Tsuji, W. *et al.* Simple and longstanding adipose tissue engineering in rabbits. *Journal of artificial organs : the official journal of the Japanese Society for Artificial Organs* **16**, 110–114, doi:10.1007/s10047-012-0670-4 (2013).
12. Ogino, S. *et al.* De novo adipogenesis using a bioabsorbable implant without additional cells or growth factors. *Journal of tissue engineering and regenerative medicine* **14**, 920–930, doi:10.1002/term.3041 (2020).
13. Ogino, S. *et al.* Development of a novel bioabsorbable implant that is substituted by adipose tissue in vivo. *Journal of tissue engineering and regenerative medicine* **12**, 633–641, doi:10.1002/term.2482 (2018).
14. Chang, K. H., Liao, H. T. & Chen, J. P. Preparation and characterization of gelatin/hyaluronic acid cryogels for adipose tissue engineering: in vitro and in vivo studies. *Acta biomaterialia* **9**, 9012–9026, doi:10.1016/j.actbio.2013.06.046 (2013).
15. Choi, J. H. *et al.* Adipose tissue engineering for soft tissue regeneration. *Tissue engineering. Part B, Reviews* **16**, 413–426, doi:10.1089/ten.TEB.2009.0544 (2010).

16. Harms, M. J. *et al.* Mature Human White Adipocytes Cultured under Membranes Maintain Identity, Function, and Can Transdifferentiate into Brown-like Adipocytes. *Cell reports* **27**, 213–225 e215, doi:10.1016/j.celrep.2019.03.026 (2019).
17. Huber, B., Borchers, K., Tovar, G. E. & Kluger, P. J. Methacrylated gelatin and mature adipocytes are promising components for adipose tissue engineering. *Journal of biomaterials applications* **30**, 699–710, doi:10.1177/0885328215587450 (2016).
18. Louis, F., Kitano, S., Mano, J. F. & Matsusaki, M. 3D collagen microfibers stimulate the functionality of preadipocytes and maintain the phenotype of mature adipocytes for long term cultures. *Acta biomaterialia* **84**, 194–207, doi:10.1016/j.actbio.2018.11.048 (2019).
19. O'Halloran, N. A., Dolan, E. B., Kerin, M. J., Lowery, A. J. & Duffy, G. P. Hydrogels in adipose tissue engineering-Potential application in post-mastectomy breast regeneration. *Journal of tissue engineering and regenerative medicine*, doi:10.1002/term.2753 (2018).
20. Zhu, Y., Kruglikov, I. L., Akgul, Y. & Scherer, P. E. Hyaluronan in adipogenesis, adipose tissue physiology and systemic metabolism. *Matrix biology : journal of the International Society for Matrix Biology*, doi:10.1016/j.matbio.2018.02.012 (2018).
21. Hossain, M. G. *et al.* Compressive force inhibits adipogenesis through COX-2-mediated down-regulation of PPARgamma2 and C/EBPalpha. *Journal of bioscience and bioengineering* **109**, 297–303, doi:10.1016/j.jbiosc.2009.09.003 (2010).
22. Yang, X. *et al.* Mechanical stretch inhibits adipogenesis and stimulates osteogenesis of adipose stem cells. *Cell proliferation* **45**, 158–166, doi:10.1111/j.1365-2184.2011.00802.x (2012).
23. Chhaya, M. P., Balmayor, E. R., Hutmacher, D. W. & Schantz, J. T. Transformation of Breast Reconstruction via Additive Biomanufacturing. *Scientific reports* **6**, 28030, doi:10.1038/srep28030 (2016).
24. Rehnke, R. D. *et al.* Breast Reconstruction Using a Three-Dimensional Absorbable Mesh Scaffold and Autologous Fat Grafting: A Composite Strategy Based on Tissue-Engineering Principles. *Plastic and reconstructive surgery* **146**, 409e-413e, doi:10.1097/PRS.0000000000007172 (2020).
25. Ikada, Y. & Tsuji, H. Biodegradable polyesters for medical and ecological applications. *Macromolecular Rapid Communications* **21**, 117–132, doi:10.1002/(sici)1521-3927(20000201)21:3<117::aid-marc117>3.0.co;2-x (2000).
26. Choi, M. *et al.* The volumetric analysis of fat graft survival in breast reconstruction. *Plastic and reconstructive surgery* **131**, 185–191, doi:10.1097/PRS.0b013e3182789b13 (2013).
27. Fedorov, A. *et al.* 3D Slicer as an image computing platform for the Quantitative Imaging Network. *Magn Reson Imaging* **30**, 1323–1341, doi:10.1016/j.mri.2012.05.001 (2012).

Tables

Table 1. Volume of the implant aggregate and the newly-formed adipose tissue

	Time after implantation			
	Post-implantation (N = 2)	1 Month (N = 2)	3 Months (N = 2)	6 Months (N = 2)
Implant aggregate (cm^3)	28.35 (28.23-28.49)	24.49 (24.39-24.58)	20.86 (18.96-22.77)	18.00 (16.48-19.50)
Newly-formed adipose tissue (cm^3)		0.01 (0-0.02)	0.43 (0.32-0.54)	3.94 (3.52-4.36)

Data expressed as mean (range).

Figures

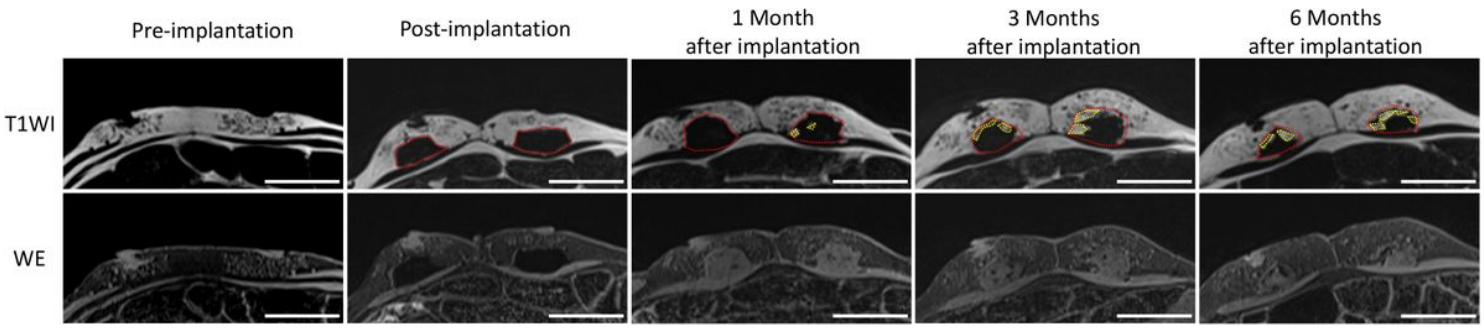

Figure 1

Magnetic resonance imaging evaluation of the volume of the implant aggregate and the newly-formed adipose tissue The red dotted lines indicate the area of the implant aggregate, and the yellow dotted lines indicate the area of newly-formed adipose tissue. The areas of the implant aggregates were confirmed at all time points. The newly-formed adipose tissue was identified as hyperintense in the T1-weighted images and the hypointense in water excitation images at 1, 3, and 6 months after implantation. Scale bar: 5 cm.

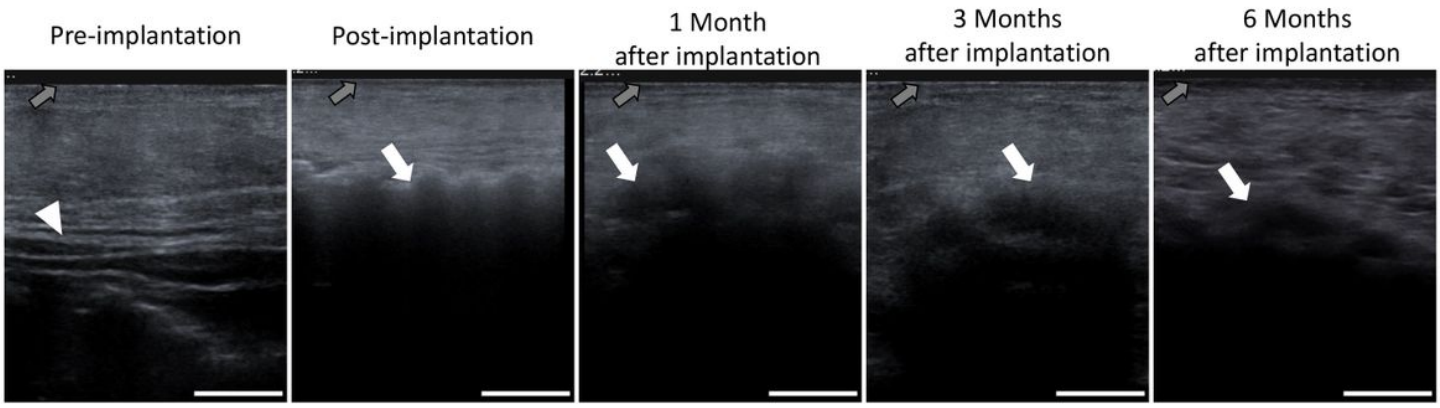

Figure 2

Ultrasound evaluation of the implant aggregate The outer surface of the implant aggregate was defined immediately after implantation, but became less distinguished over time. The acoustic shadow of the outer surface diminished over time. The hyperechoic area was confirmed in the internal space of the implant aggregate one month after implantation. The white arrowhead indicates the deep fascia. The white arrows indicate the outer surface of the implant aggregate. The gray arrows indicate the epidermis. Scale bar: 1cm.

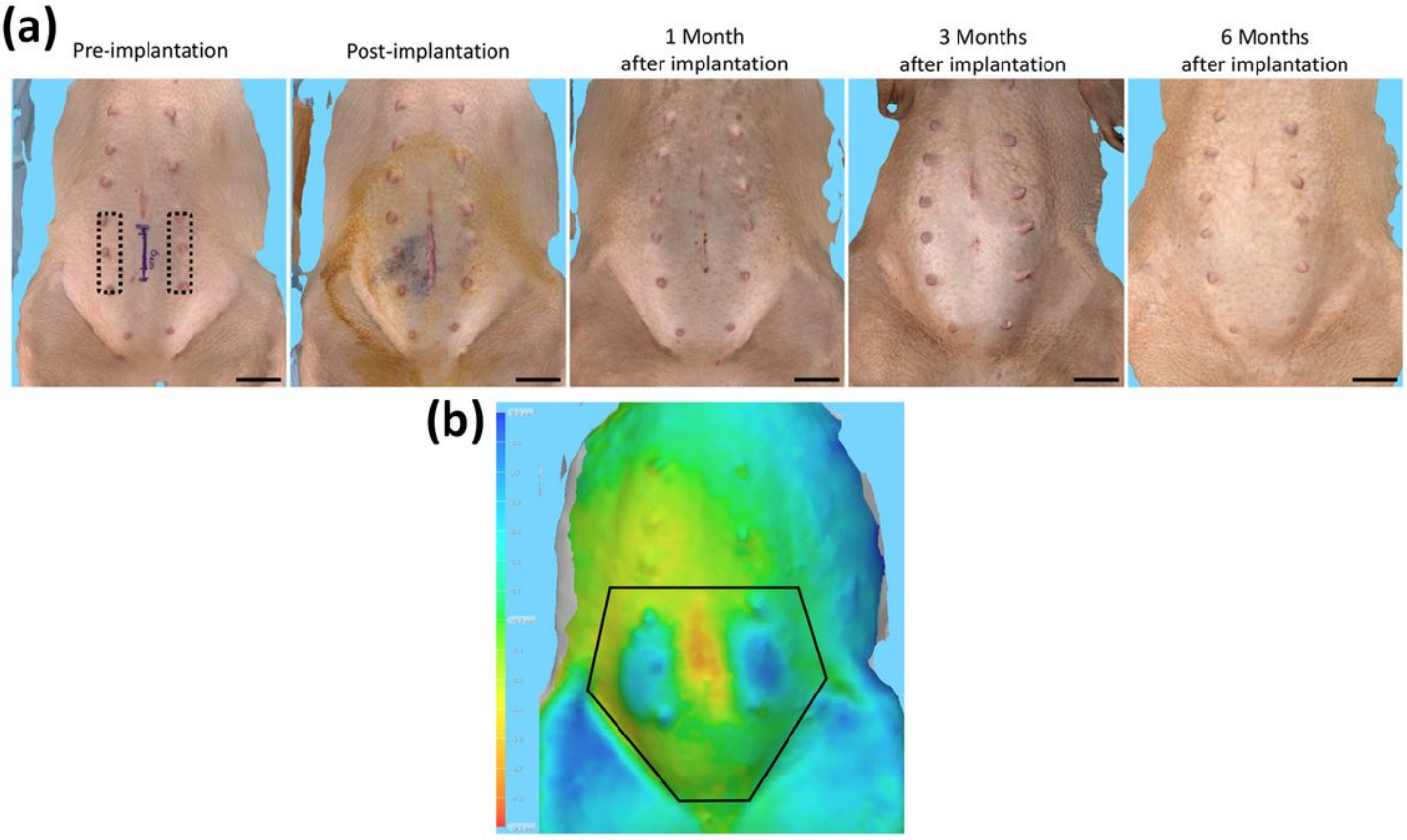

Figure 3

Three-dimensional imaging evaluation (a) The 3D imaging at the abdominal side shows a slight bulge at 1, 3, and 6 months after implantation. The blue line represents the 6-cm incision. The black-dotted area shows where the implant aggregate was inserted. Scale bar: 5 cm. (b) The change between pre-implantation and post-implantation are shown. The black line indicates the area of the evaluated volume change. The volume in post-implantation increased 33.15 cm3 comparing with that in pre-implantation

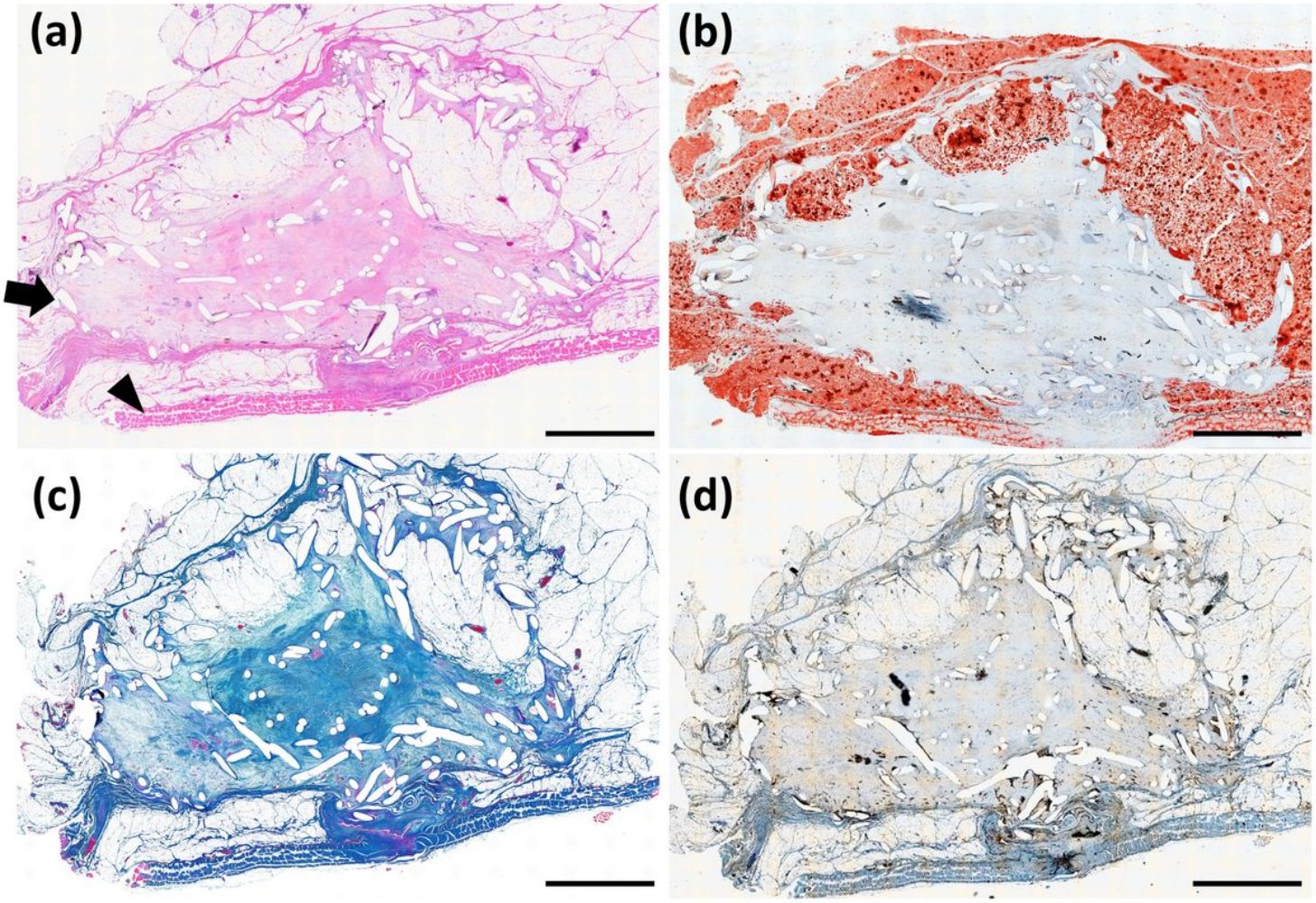

Figure 4

Histological evaluation of the implant aggregate Light micrographs of (a) hematoxylin-eosin (H&E)-stained sections, (b) oil-red-o-stained sections, and (c) azocarmine and aniline blue (AZAN)-stained sections six months after implantation are shown. The presence of poly-L-lactic acid (PLLA) mesh is confirmed. The internal space in the implant aggregate is maintained, and the regeneration of adipose tissue and collagen fiber is confirmed. (d) Light micrographs of anti-CD31 are shown. Newly-formed capillaries are observed in the area of formed collagen fiber. The black arrowhead indicates the fascia, and the black arrow indicates the PLLA thread. Scale bar: 5 mm

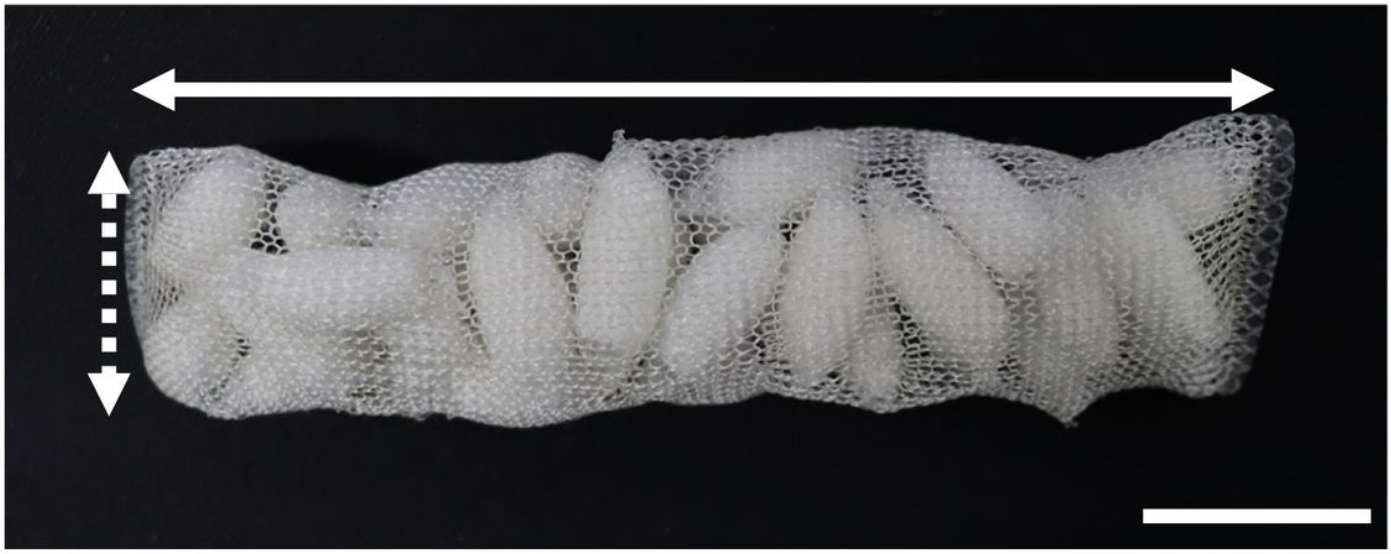

Figure 5

Poly-L-lactic acid implant aggregate The gross appearance of the poly-L-lactic acid (PLLA) implant aggregate. The dashed white arrow indicates the largest diameter of the short axis, and the solid white arrow indicates the greatest length of the long axis. Scale bar: 2